

Models of Mira variables of the Large Magellanic Cloud

Yu. A. Fadeyev*

*Institute of Astronomy, Russian Academy of Sciences, Pyatnitskaya ul. 48, Moscow, 119017
Russia*

Received September 23, 2024; revised October 24, 2024; accepted October 24, 2024

Abstract — Consistent stellar evolution and nonlinear radial stellar pulsation calculations were carried out for models of asymptotic giant branch stars with initial masses $1.5M_{\odot} \leq M_{\text{ZAMS}} \leq 3M_{\odot}$ and initial metal abundance $Z = 0.006$. All the models are shown to be either the fundamental mode or the first overtone pulsators. The lower limit of the first overtone period increases with increasing mass of the Mira model from $\Pi_{1,\text{min}} \approx 80$ days for $M = 1.3M_{\odot}$ to $\Pi_{1,\text{min}} \approx 120$ days for $M = 2.6M_{\odot}$. The upper limit of the first overtone period and lower limit of the fundamental mode period depend on the stellar structure during mode switching and range from $\Pi_{1,\text{max}} = 130$, $\Pi_{0,\text{min}} = 190$ days for $M = 0.96M_{\odot}$ to $\Pi_{1,\text{max}} = 210$, $\Pi_{0,\text{min}} = 430$ days for $M = 2.2M_{\odot}$. The slope of the theoretical period–luminosity relation of Mira variables perceptibly increases with decreasing Z . Fourier spectra of the kinetic energy of twelve hydrodynamic models show a split of the fundamental mode maximum into several equidistant components. Frequency intervals between split components fall within the range $0.03 \leq \Delta\nu/\nu_0 \leq 0.1$. The superposition of radial oscillations with the fundamental mode splitting leads to the long–term amplitude variations with the cycle length from 10 to 30 times longer than the fundamental mode period. A more thorough analysis of hydrodynamic models is required for understanding the origin of the principal pulsation mode splitting.

Keywords: *stellar evolution; stellar pulsation; stars: variable and peculiar*

*E-mail: fadeyev@inasan.ru

INTRODUCTION

The period–luminosity relation of Mira variables discovered by Glass and Lloyd Evans (1981) from IR observations of red giants in the Large Magellanic Cloud (LMC) is now a reliable tool for determination of interstellar distance scale (Glass and Feast 1982; Feast 1984; Whitelock et al. 2000; 2008; Iwanek et al. 2021). Moreover, observations of long period variables in neighbouring galaxies allow us to expand limits of the usage of Mira variables as distance indicators to the Local Group of galaxies (Mould 2004; Whitelock et al. 2013; Huang et al. 2018; Yan et al. 2018). At the same time, despite of significant progress in observations of Mira variables their physical nature is still poorly understood. First of all, one should note uncertainties in the theory of late stages of stellar evolution because the Mira variables are the stars of the asymptotic giant branch undergoing thermal pulses (i.e. TP–AGB stars) in the helium shell source (Iben and Renzini 1983; Herwig 2005). Another obstacle is that the application of the linear theory of stellar pulsation may lead to dubious results because of the large oscillation amplitude in Mira variables. Strong shock waves appearing because of the large radial displacement of outer layers are responsible for significant redistribution of gas density in the stellar atmosphere and favour dust grain formation (Willson 2000). Models of red giant nonlinear pulsations computed with the numerical methods of radiation hydrodynamics encounter significant difficulties when the expansion velocity of outer layers exceeds the local escape velocity (Wood 1974; Tuchman et al. 1978; Olivier and Wood 2005).

Among the few studies devoted to nonlinear oscillations of red giants we have to note the paper by Trabucchi et al. (2021) where a great deal of hydrodynamic models with various stellar masses, radii and luminosities are successfully compared with Mira variables of the LMC. Unfortunately, a significant shortcoming of this study is due to the fact that the initial conditions required for solution of the equations of hydrodynamics were calculated with the carbon core mass – luminosity relation (Trabucchi et al. 2019) rather than from the stellar evolution computations. In particular, this method does not allow to obtain the theoretical period–luminosity relation ($\Pi - L$).

Theoretical estimates of various characteristics of Mira variables as well as the $\Pi - L$ relation can be obtained only on the basis of consistent computations of stellar evolution and nonlinear stellar pulsations when initial conditions required for solution of the equations of hydrodynamics describing stellar oscillations are determined using computed in advance evolutionary sequence models. This method was earlier applied by the author (Fadeyev 2023) to determine the theoretical period–radius and period–luminosity relations of Mira models with solar metallicity ($Z = 0.014$).

Below we present the results of consistent computations of stellar evolution and nonlinear

radial stellar pulsations of Mira models with initial metal abundance $Z = 0.006$ corresponding to the recent observational estimates of metallicity of LMC stars (Rolleston et al. 2002; Cole et al. 2005). The goal of this study implies the solution of the following problems:

- Determination of the stellar evolution phases corresponding to the certain radial oscillation mode.
- Estimation of period ranges for each of oscillation modes.
- Determination of the theoretical $\Pi - L$ relation for Mira models with the metal abundance $Z = 0.006$ and comparison with results obtained earlier for $Z = 0.014$ (Fadeyev 2023).

Looking ahead, it should be noted that during this work we found that limit cycle oscillations of some hydrodynamic models are characterized by frequency split of the principal oscillation mode and show cyclic amplitude variations on the time scale by an order of magnitude longer than the pulsation period. In the final part of this paper we discuss both main features of this phenomenon and possible explanation of the long secondary periodicity (LSP) discovered more than twenty years ago in pulsating red giants of LMC (Wood et al. 1999; Wood 2000) but has not been explained yet.

EVOLUTIONARY SEQUENCES OF AGB STARS

Stellar evolution from the main sequence up to the final AGB stage was computed with the program MESA version r15140 (Paxton et al. 2019). Details of computations and required parameters are discussed in our previous paper (Fadeyev 2023). Altogether, we computed 9 evolutionary sequences with zero age main sequence masses $1.5M_{\odot} \leq M_{\text{ZAMS}} \leq 3M_{\odot}$ for initial abundances of helium and heavier elements (metals) $Y = 0.28$ and $Z = 0.006$.

The main feature of the TP–AGB evolutionary stage is that the luminosity of the helium shell source experiences quasi–periodic increases accompanied by significant variations of the stellar radius and luminosity that are responsible for secular changes of the pulsation period in some Mira variables (Wood and Zarro 1981). The typical plot of luminosity variations during $\approx 2.3 \times 10^6$ yr of the TP–AGB phase in the red giant with initial mass $M_{\text{ZAMS}} = 2M_{\odot}$ is shown in Fig. 1.

The carbon core mass – luminosity relation for the TP–AGB evolutionary sequence $M_{\text{ZAMS}} = 2M_{\odot}$ determined by the weighted least squares with weights proportional to the evolution time can be approximately written as

$$L/L_{\odot} = 4.255 \times 10^4 (M_{\text{C}} - 0.426) \quad (1)$$

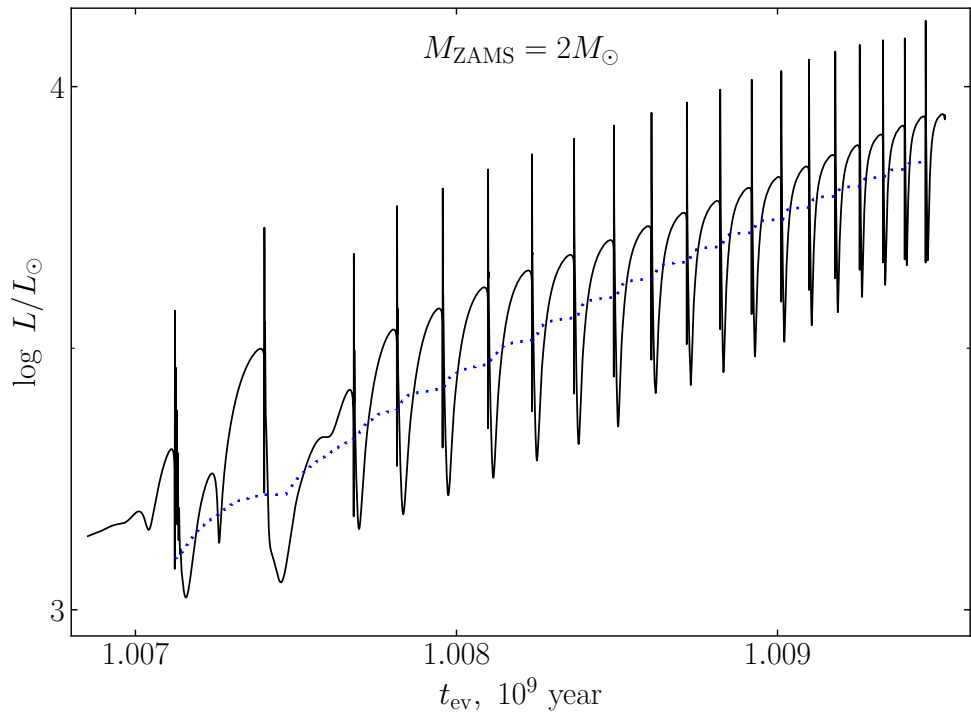


Figure 1. Luminosity variations during the TP–AGB evolutionary stage in the star with initial mass $M_{\text{ZAMS}} = 2M_{\odot}$. The carbon core mass – luminosity relation (1) is shown by the dotted line.

and is shown in Fig. 1 by the dotted line which deviates from the straight line due to non-monotonic growth of the carbon core. As seen in Fig. 1, each thermal flash is accompanied by significant variations of the stellar luminosity so that the use of (1) for calculation of initial conditions will inevitably lead to wrong results.

In the present study the initial conditions required for the solution of the equations of hydrodynamics describing stellar pulsations were calculated using the selected TP–AGB stellar models. One should bear in mind that not all models of the TP–AGB evolutionary sequence can be used for calculation of initial conditions since the applicability of the theory of stellar pulsation is restricted to the conditions of hydrostatic and thermal equilibrium. The first of these conditions is fulfilled in all evolutionary models because it is a part of the solution of stellar structure equations. At the same time during some evolutionary phases the thermal imbalance can appear in the stellar envelope when the gravitational energy changes because of contraction or expansion of the star. In particular, such changes take place in TP–AGB red giants during short-term maxima of the helium shell source luminosity. The duration of the thermal imbalance in Mira variables does not exceed a few percent of the interflash interval (Fadeyev 2023) and on the luminosity plot in Fig. 1 this time interval is in the close vicinity of luminosity peaks. In the present study the calculations of initial conditions were restricted to

the models of evolutionary sequences corresponding to the monotonic luminosity growth (see Fig. 1) when the condition of thermal equilibrium is fulfilled to high accuracy.

It should be noted that the consistency between the initial conditions and calculations of stellar pulsation is provided not only by distributions of the radius, luminosity and other variables with respect to the Lagrangian mass coordinate but also by the same elemental abundances within the stellar envelope. This condition is of importance during the TP–AGB stage because of changes of elemental abundances after the onset of the 3rd dredge–up from the helium–burning shell.

HYDRODYNAMIC MODELS OF MIRAS

The basic equations of radiation hydrodynamics and time–dependent convection we used for calculation of radial oscillations in Miras are discussed in one of our preceding papers (Fadeyev 2013). There are two types of the Cauchy problem solution for nonlinear stellar pulsations. The first describes the amplitude growth and subsequent transition to oscillations with the constant amplitude. The second describes decaying oscillations indicating that the stellar model is stable against radial pulsations. For both types of the solution we calculated the pulsation period Π using the discrete Fourier transform of the kinetic energy of stellar pulsation motions. In the case of pulsationally unstable models the period was calculated after attainment of limiting amplitude whereas in the case of decaying oscillations the period was determined for the whole interval of the solution. The relative error of the period determination does not exceed $\approx 1\%$.

Results of consistent stellar evolution and nonlinear stellar pulsation calculations for the evolutionary sequence $M_{\text{ZAMS}} = 2M_{\odot}$ are illustrated in Fig. 2. For the sake of convenience the results are plotted for thermal flashes with even numbers $12 \leq i_{\text{TP}} \leq 20$ and the evolution time t_{ev} is set to zero at the maximum peak of the helium–shell luminosity. Circles and triangles mark hydrodynamic models pulsating in the fundamental mode and first overtone whereas open symbols correspond to models with decaying oscillations.

As seen in Fig. 2, during the initial TP–AGB stage (i.e. for $i_{\text{TP}} < 12$) the models of the evolutionary sequence $M_{\text{ZAMS}} = 2M_{\odot}$ are stable against the radial oscillations. However the hydrogen and helium ionization zones, where pulsations are driven, expand as the luminosity increases so that the star begins to pulsate after the thermal pulse $i_{\text{TP}} = 12$.

At the beginning of oscillations the star is the first overtone pulsator because the inner boundary of the hydrogen and helium ionization zones locate above the node of the first overtone. The radius of the node is $r_{\text{n}} \approx 0.77R$, where R is the surface radius of the evolution model. The duration of the evolutionary stage when the star pulsates increases with increasing number of the thermal flash because of higher stellar luminosity and the larger size of ionization zones. As seen in Fig. 2a, for $12 \leq i_{\text{TP}} \leq 16$ the star pulsates in the first overtone. For $i_{\text{TP}} = 18$ the

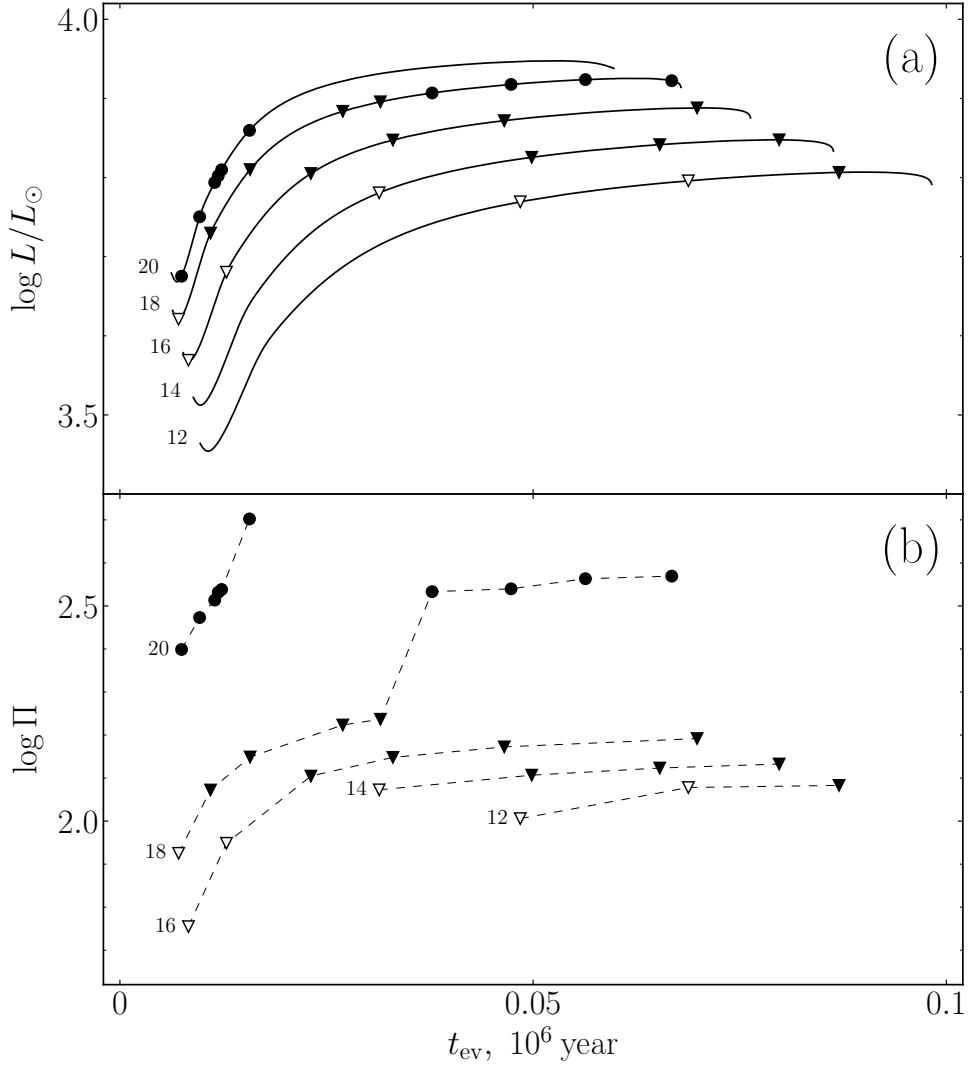


Figure 2. Variations of the luminosity (a) and period of radial oscillations (b) after the helium flash in models of the evolutionary sequence $M_{\text{ZAMS}} = 2M_{\odot}$ during luminosity growth. On the left of the plots the thermal flash number i_{TP} is marked. The evolution time is set to zero at the luminosity peak of the helium shell source. Hydrodynamic models pulsating in the fundamental mode and first overtone are shown by circles and triangles. The filled and open symbols correspond to models of pulsating stars and to those with decaying oscillations.

growth of stellar luminosity is accompanied by pulsation mode switch from the first overtone to the fundamental mode since the inner boundary of ionization zones plunges below the first overtone node. The thermal flash $i_{\text{TP}} = 20$ is the last in this evolutionary sequence. The low stellar mass ($M \leq 1.26M_{\odot}$) and increasing luminosity are responsible for further increase of the pulsation amplitude and less regular oscillations.

As seen in Fig. 2b, during the final TP–AGB stage of the stellar evolution the range of periods variation during the thermal pulse cycle significantly increases. For example, during

the cycle $i_{\text{TP}} = 18$ the pulsation periods changes from ≈ 120 days (oscillations in the first overtone) to ≈ 610 days (fundamental mode pulsations).

The pulsation period monotonically increases during each cycle of thermal instability so that we can evaluate the minimum and maximum values of the first overtone and fundamental mode periods for each cycle of thermal instability and ultimately to determine the limits of period changes for the evolutionary sequence with initial mass M_{ZAMS} . In particular, the first overtone period at the edge of pulsational instability is determined as the mean value of the periods of two adjacent models one of which shows decaying oscillations whereas another is unstable against radial pulsations. The upper limit of the first overtone period and the lower limit of the fundamental mode period are evaluated in vicinity of the mode switch (see, for example, the plot $i_{\text{TP}} = 18$ in Fig. 2b):

$$\Pi_{1,\text{max}} = \frac{1}{2}(\Pi_1 + \frac{1}{2}\Pi_0), \quad (2)$$

$$\Pi_{0,\text{min}} = \frac{1}{2}(2\Pi_1 + \Pi_0), \quad (3)$$

where Π_1 and Π_0 are the first overtone and fundamental mode periods of two adjacent models. In relations (2) and (3) we used the fact that the periods of the first overtone and fundamental mode relate as $\Pi_1/\Pi_0 = 1/2$.

Rough estimates of the limit values of pulsation periods in Mira models are shown in Fig. 3 as a function of the initial mass of the evolutionary sequence M_{ZAMS} . It should be noted that non-monotonic increase in $\Pi_{1,\text{max}}$ and $\Pi_{0,\text{min}}$ seems to be due to insufficiently dense grid of hydrodynamic models for $2M_{\odot} \leq M_{\text{ZAMS}} \leq 2.4M_{\odot}$.

PERIOD–LUMINOSITY RELATION

As shown above, during a cycle of thermal instability the pulsation period varies within a wide range so that pulsations with the same period can appear at different values of i_{TP} . Therefore the luminosity of stars pulsating with nearly the same period can vary due to monotonic growth of the carbon core mass as the star ascends the AGB and models of the same evolutionary sequence are dispersed in the $\Pi - L$ diagram. This feature is illustrated in Fig. 4, where the period–luminosity diagram is shown for hydrodynamic models of the evolutionary sequence $M_{\text{ZAMS}} = 1.5M_{\odot}$ pulsating in the first overtone ($6 \leq i_{\text{TP}} \leq 9$) and in the fundamental mode ($8 \leq i_{\text{TP}} \leq 10$). As can be seen from these plots, the values of $\log \Pi$ and $\log L$ agree with the linear fit to good accuracy for a fixed value of i_{TP} but the fitting straight lines are shifted to the right along the horizontal axis because of stellar mass decrease. Stellar oscillations in the fundamental mode take place during stronger mass loss when deviation of $\log \Pi$ and $\log L$ from the linear fit becomes more appreciable.

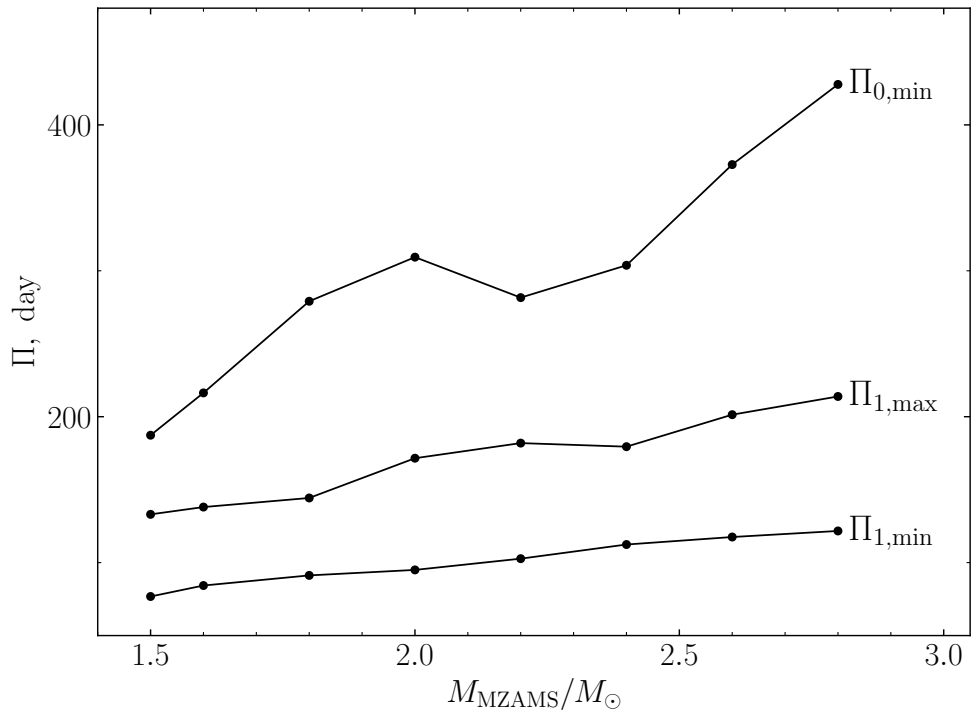


Figure 3. The minimum and maximum values of the first overtone period $\Pi_{1,\text{min}}$ and $\Pi_{1,\text{max}}$ and the minimum value of the fundamental mode period $\Pi_{0,\text{min}}$ against the initial stellar mass M_{ZAMS} .

In the present study we computed 195 hydrodynamic models of Mira variables pulsating in the first overtone and 90 models pulsating in the fundamental mode. The theoretical $\Pi - L$ relations for the fundamental mode and first overtone are shown in Fig. 5, where the different symbols correspond to models of evolutionary sequences that are listed in the upper left corner of Fig. 5.

The solid lines in Fig. 5 represent the linear fits of $(\log L, \lg \Pi_0)$ and $(\log L, \lg \Pi_1)$ values.

$$M_{\text{bol}} = -4.328 \log \Pi_0 + 5.967, \quad (4)$$

$$M_{\text{bol}} = -3.820 \log \Pi_1 + 3.306. \quad (5)$$

A noticeable scatter of points around the straight lines (4) and (5) is due to different values of the carbon core mass of hydrodynamic models.

The diagram in Fig. 5 as well as relations (4) and (5) correspond to the absolute bolometric magnitude M_{bol} whereas all empirical period–luminosity relations of Mira variables in the LMC were determined for near-infrared magnitudes. For example, the slope of the $\Pi - L$ relation evaluated from observation in the K passband of 53 Mira variables in the LMC with periods from 116 to 413 days is $\rho = -3.69$ (Whitelock et al. 2008). According to Josselin et al. (2000) the bolometric magnitudes of AGB stars and their K magnitudes, corrected for interstellar

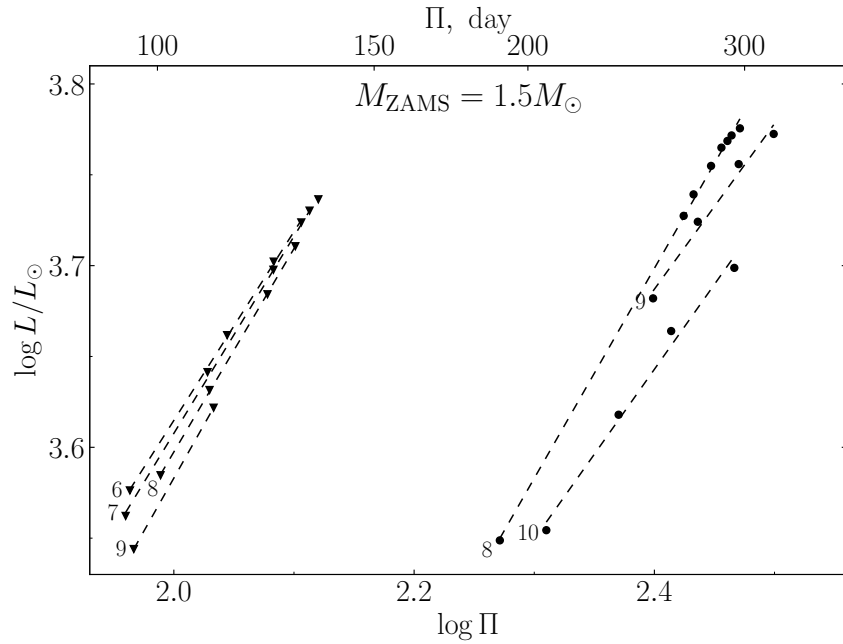


Figure 4. Hydrodynamic models of the evolutionary sequence $M_{\text{ZAMS}} = 1.5M_{\odot}$ on the diagram period – luminosity. Circles and triangles represent the fundamental mode and first overtone pulsators. Dashed lines represent the least square fit for models of the same thermal cycle. Index of the thermal cycle i_{TP} is shown on the left at each dependence.

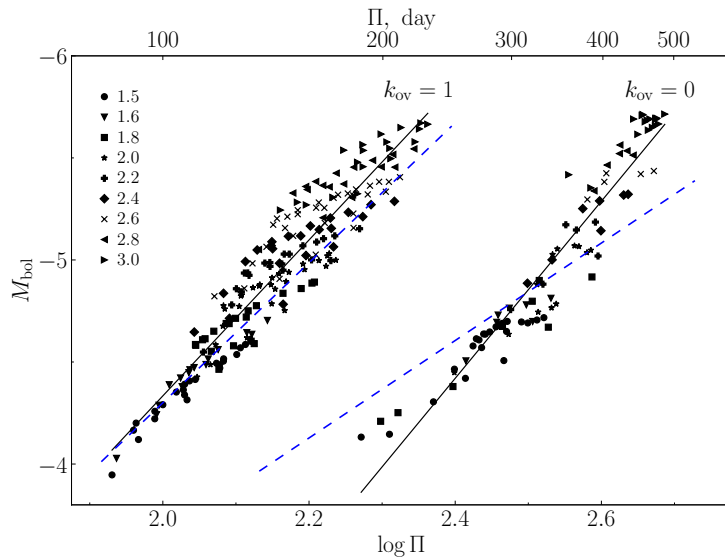


Figure 5. Period–luminosity relations for the fundamental mode ($k_{\text{ov}} = 0$) and first overtone ($k_{\text{ov}} = 1$) pulsators with metal abundance $Z = 0.006$. Different symbols represent the models of evolutionary models with $1.5M_{\odot} \leq M_{\text{ZAMS}} \leq 3M_{\odot}$. The solid lines represent linear fits (4) and (5), whereas the dashed lines show the linear fits obtained for Mira variable models with $Z = 0.014$ (Fadeyev 2023).

extinction, relate as

$$m_{\text{bol}} \simeq m_{\text{K}} - 3. \quad (6)$$

There are two ways to explain the difference between the slope -4.33 of theoretical relation (4) and the value -3.69 of the empirical relation by Whitelock et al. (2008). First, we have to assume that the bolometric correction relating m_{bol} and m_{K} is not constant. Second, the better agreement between the theory and observations can probably be obtained for the larger metal abundance Z . In particular, the dashed lines in Fig. 5 that represent linear fits of the period–luminosity relation for models with metal abundance $Z = 0.014$ have smaller slope (-2.39 for fundamental mode pulsators). Therefore, the small increase of metal abundance in comparison with $Z = 0.006$ can probably improve agreement with observations.

MODELS OF MIRA VARIABLES WITH SECONDARY PERIODICITY

Among nearly three hundred models of Mira variables considered in the present study we found twelve hydrodynamic models where the limit amplitude oscillations were accompanied by the long–term secondary periodicity. The example of radial pulsations with secondary periodicity is shown in Fig. 6, where variations of maximum values of the pulsation kinetic energy $E_{\text{K,max}}$ are plotted against the number of fundamental mode periods t/Π_0 for the Mira variable model with the mass $M = 2.49M_{\odot}$ and period $\Pi_0 = 469$ days. In models without the secondary periodicity the maximum of kinetic energy after attainment of the limiting amplitude is independent of time t whereas the model in Fig. 6 shows cyclic variations of the pulsation amplitude on the time scale nearly 30 times longer than the period of radial oscillations ($\Pi_{\text{s}}/\Pi_0 = 31$). Calculations of nonlinear pulsations for the model shown in Fig. 6 we carried out for the long enough time interval ($t \sim 2.5 \times 10^3 \Pi_0$) but nevertheless attempts to detect any secular changes of amplitude variations failed.

To exclude any doubts that the secondary periodicity is an computational artefact arising due to the discrete nature of the numerical model we carried out the nonlinear pulsation calculations for the same model but with the doubled number of mass zones. Results of calculations are shown in Fig. 7 where the kinetic energy power spectra are plotted for two cases of the number of mass zones: $N = 600$ and $N = 1200$. Both spectra were computed for the solution obtained on the time interval $t/\Pi_0 \approx 1.3 \times 10^3$. An insignificant difference between these Fourier spectra allows us to conclude that long–term cyclic variations of the pulsation amplitude are not the computational artefact because they are almost independent of the number of mass zones of the hydrodynamic model.

An essential feature of the plots in Fig. 7 is that the principal maximum is split into several equidistant frequency components, so that their superposition is responsible for appearance of

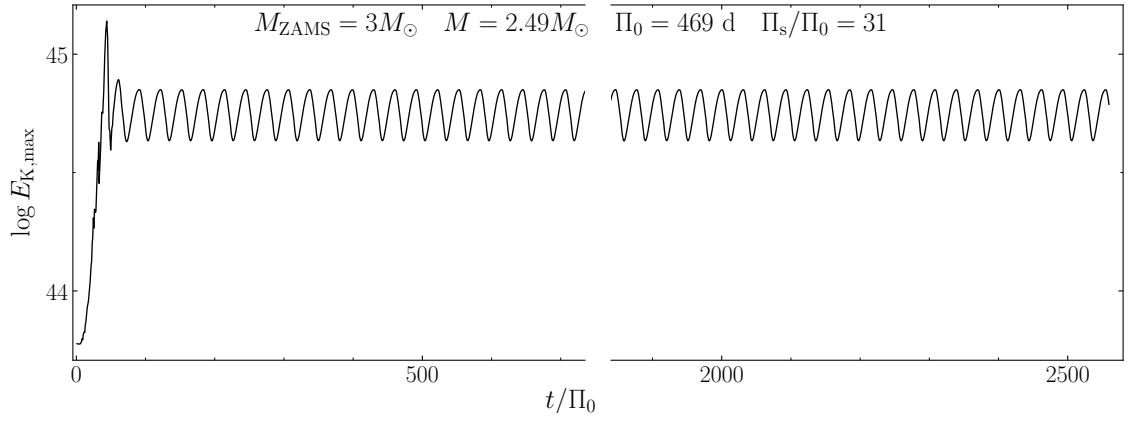


Figure 6. Variations of maximum values of the kinetic energy of pulsations motions in the model with mass $M = 2.49M_{\odot}$ and the period $\Pi = 469$ d (the evolutionary sequence $M_{\text{ZAMS}} = 3M_{\odot}$).

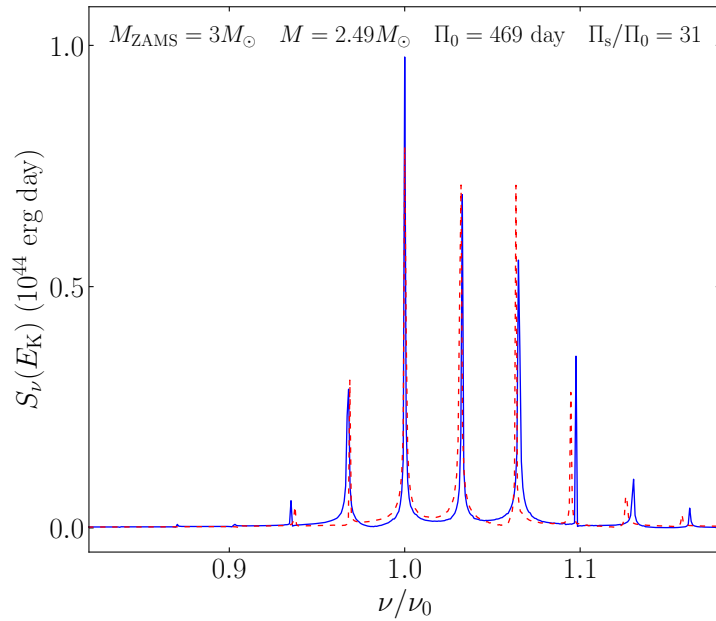


Figure 7. The power spectrum of the pulsation kinetic energy $S_{\nu}(E_K)$ in the vicinity of the fundamental mode frequency $\nu_0 = 1/\Pi_0$ of the hydrodynamic model shown in Fig. 6 (solid line). The power spectrum of the model with the doubled number of Lagrangian mass zones ($N = 1200$) is shown by the dashed line.

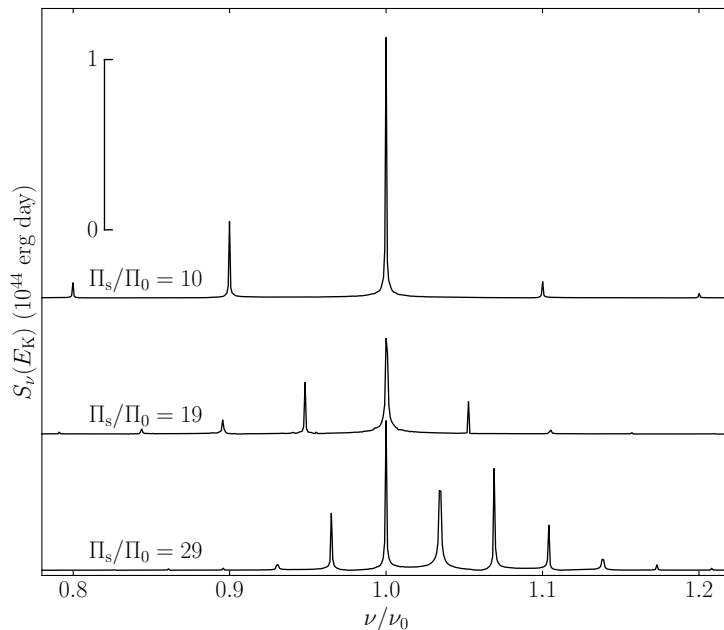


Figure 8. The kinetic energy power spectra $S_\nu(E_K)$ in the vicinity of the principal mode frequency $\nu_0 = 1/\Pi_0$ for three hydrodynamic models with ratios $\Pi_s/\Pi_0 = 10, 19$ and 29 .

long-term cyclic variations of the pulsation amplitude. The ratio Π_s/Π_0 depends on the both the amplitude of peaks and frequency interval between peaks. This is clearly seen in Fig. 8 from power spectrum plots of three hydrodynamic models with period ratios $\Pi_s/\Pi_0 = 10, 19$ and 29 .

Main characteristics of hydrodynamic models with secondary periodicity are listed in Table 1 in order of increasing frequency split $\Delta\nu/\nu_0$ which corresponds to decreasing period ratio Π_s/Π . All models in Table 1 are the fundamental mode pulsators.

Initially the secondary periodicity was found occasionally in several hydrodynamic models. To clarify the connection between this phenomenon and the evolutionary changes of stellar structure we calculated a few more hydrodynamic models of the evolutionary sequence $M_{\text{ZAMS}} = 3M_\odot$. Thus, four models on the stage $i_{\text{TP}} = 8$ and three models on the stage $i_{\text{TP}} = 9$ represent two sequences of stellar models with continuous secondary periodicity. The duration of the secondary periodicity stage is $t_{\text{sp}} \approx 5.6 \times 10^3$ yr for $i_{\text{TP}} = 8$ and $t_{\text{sp}} \approx 1.1 \times 10^3$ yr for $i_{\text{TP}} = 9$. The interflash interval is $\Delta t_{\text{TP}} \approx 2.2 \times 10^4$ yr so that the duration of the second periodicity is as long as 25% and 5%, respectively.

CONCLUSIONS

Consistent calculations of stellar evolution and nonlinear stellar oscillations done in the present work allow us to clarify some details about Mira variables. Here we mention them.

Table 1. Main characteristics of hydrodynamic models with secondary periodicity.

$M_{\text{ZAMS}}/M_{\odot}$	M/M_{\odot}	i_{TP}	Π , day	Π_{s}/Π	$\Delta\nu/\nu_0$
3.0	2.490	8	469.2	30.8	0.0323
3.0	2.423	9	461.5	28.9	0.0350
3.0	2.476	8	472.5	28.3	0.0351
3.0	2.461	8	474.4	27.0	0.0372
3.0	2.452	8	472.4	27.0	0.0374
3.0	2.420	9	467.4	26.8	0.0374
3.0	2.417	9	471.9	25.7	0.0390
2.8	2.181	12	431.6	22.8	0.0441
2.6	1.969	14	401.9	19.2	0.0521
3.0	2.010	11	385.1	15.7	0.0641
2.8	2.055	13	405.4	14.3	0.0709
3.0	2.234	10	476.6	10.0	0.1000

In the early TP–AGB stage (i.e. during the first several thermal flashes) the red giant remains stable against radial pulsations. Evolutionary increase in the luminosity is accompanied by extension of the hydrogen and helium ionizing zones where pulsations are excited. Initially oscillations arise due to instability of the first overtone since the inner boundary of ionization zones locates above the node of the first overtone with radius $r_{\text{n}}/R \approx 0.77$, where R is the outer radius of the evolution model. Models pulsating in higher order overtones were not found. Enough dense grid of hydrodynamic models allowed us to determine the lower limit of the first overtone period which increases with increasing stellar mass from $\Pi_{1,\text{min}} \approx 80$ days (the stellar mass $M = 1.27M_{\odot}$, the evolutionary sequence $M_{\text{ZAMS}} = 1.5M_{\odot}$) to $\Pi_{1,\text{min}} \approx 120$ days ($M = 2.60M_{\odot}$, $M_{\text{ZAMS}} = 2.8M_{\odot}$).

The existence of the upper limit of the first overtone period $\Pi_{1,\text{max}}$ is due to the mode switch to the fundamental mode. The duration of mode switch in Mira variables comprises $\sim 10^2$ oscillation cycles (Fadeyev 2022) and in comparison with the evolution timescale of TP–AGB stars can be treated as an instant process. Moreover, in the vicinity of the mode switch the periods of the first overtone and fundamental mode relate as $\Pi_1/\Pi_0 = 1/2$ so that together with the upper limit of the first overtone we obtain the estimate of the lower limit of the fundamental mode period. In the evolutionary sequences $1.5M_{\odot} \leq M_{\text{ZAMS}} \leq 2.8M_{\odot}$ these limit values increase with increasing stellar mass M from $\Pi_{1,\text{max}} = 130$ and $\Pi_{0,\text{min}} = 190$ days for $M = 0.96M_{\odot}$ to $\Pi_{1,\text{max}} = 210$ and $\Pi_{0,\text{min}} = 430$ days for $M = 2.2M_{\odot}$.

Comparison of the results of the present work with those obtained earlier for Mira variable models with $Z = 0.014$ (Fadeyev 2023) allows us to conclude that the slope of the theoretical period–luminosity relation increases with decreasing Z . The metal dependence of the slope of empirical period–luminosity relations have been recently demonstrated by Chibueze et al. (2020).

The theoretical period–luminosity relation was determined in the present study for bolometric magnitudes and its slope (-4.33) is larger than the observational estimate in the K passband $\rho = -3.69$ (Whitelock et al., 2008). One of the reasons of this difference might be the non–constant bolometric correction which remains fairly uncertain. On the other hand, the smaller slope of the theoretical dependence can probably be obtained for $Z = 0.008$ but this conclusion should be checked based of additional stellar evolution and stellar pulsation computations.

Among nearly three hundred hydrodynamic Mira variable models calculated in the present study twelve of them were found to have the kinetic energy power spectrum with split components in the vicinity of the fundamental mode frequency. In each model the frequency components are equidistant and for calculated hydrodynamic models are in the range $0.03 \leq \Delta\nu/\nu_0 \leq 0.10$, where ν_0 is the frequency of the principal component. The superposition of oscillations in the hydrodynamic models with the split kinetic energy spectrum leads to the long–term cyclic variations of the pulsation amplitude. The ratio of the secondary period Π_s to the fundamental mode period Π_0 depends of the frequency $\Delta\nu$ and ranges from $\Pi_s/\Pi = 10$ for $\Delta\nu/\nu_0 = 0.10$ to $\Pi_s/\Pi = 31$ for $\Delta\nu/\nu_0 = 0.03$. The physical nature of the split of the kinetic energy spectrum remains, unfortunately, unclear. To comprehend the origin of the pulsation spectrum split in radially pulsating stars one should undertake a more detailed analysis of hydrodynamic models. Perhaps this will allow us to understand the nature of the long secondary periodicity in Mira variables.

REFERENCES

1. J.O. Chibueze, R. Urago, T. Omodaka, Y. Morikawa, M.Y. Fujimoto, A. Nakagawa, T. Nagayama, T. Nagayama, K. Hirano, *Publ. Astron. Soc. Japan* **72**, 59 (2020).
2. A.A. Cole, E. Tolstoy, J.S. Gallagher, T.A. Smecker-Hane, *Astron. J.* **129**, 1465 (2005).
3. Yu.A. Fadeyev, *Astron. Lett.* **39**, 306 (2013).
4. Yu.A. Fadeyev, *Mon. Not. R. Astron. Soc.* **514**, 5996 (2022).
5. Yu.A. Fadeyev, *Astron. Lett.* **49**, 722 (2023).

6. M.W. Feast, *Mon. Not. R. Astron. Soc.* **211**, 51 (1984).
7. I.S. Glass and T. Lloyd Evans, *Nature* **291**, 303 (1981).
8. I.S. Glass and M.W. Feast, *Mon. Not. R. Astron. Soc.* **199**, 245 (1982).
9. F. Herwig, *Ann. Rev. Astron. Astrophys.* **43**, 435 (2005).
10. C.D. Huang, A.G. Riess, S.L. Hoffmann, C. Klein, J. Bloom, W. Yuan, L.M. Macri, D.O. Jones, P.A. Whitelock, S. Casertano, and R.I. Anderson, *Astrophys. J.* **857**, 67 (2018).
11. I. Iben and A. Renzini, *Ann. Rev. Astron. Astrophys.* **21**, 271 (1983).
12. P. Iwanek, I. Soszyński, and S. Kozłowski, *Astrophys. J.* **919**, 99 (2021).
13. E. Josselin, J.A.D.L. Blommaert, M.A.T. Groenewegen, A. Omont, and F.L. Li, *Astron. Astrophys.* **357**, 225 (2000).
14. J. Mould, A. Saha, and S. Hughes, *Astrophys. J. Suppl. Ser.* **154**, 623 (2004).
15. E.A. Olivier and P.R. Wood, *Mon. Not. R. Astron. Soc.* **362**, 1396 (2005).
16. B. Paxton, R. Smolec, J. Schwab, A. Gaulty, L. Bildsten, M. Cantiello, A. Dotter, R. Farmer, J.A. Goldberg, A.S. Jermyn, S.M. Kanbur, P. Marchant, A. Thoul, R.H.D. Townsend, W.M. Wolf, M. Zhang, and F.X. Timmes, *Astrophys. J. Suppl. Ser.* **243**, 10 (2019).
17. W.R.J. Rolleston, C. Trundle, and P.L. Dufton, *Astron. Astrophys.* **396**, 53 (2002).
18. M. Trabucchi, P.R. Wood., J. Montalbán, P. Marigo, G. Pastorelli, L. Girardi, *Mon. Not. R. Astron. Soc.* **482**, 929 (2019).
19. M. Trabucchi, P.R. Wood, N. Mowlavi, G. Pastorelli, P. Marigo, L. Girardi and T. Lebzelter), *Mon. Not. R. Astron. Soc.* **500**, 1575 (2021).
20. Y. Tuchman, N. Sack, and Z. Barkat, *Astrophys. J.* **219**, 183 (1978).
21. P.A. Whitelock, F. Marang, and M.W. Feast, *Mon. Not. R. Astron. Soc.* **319**, 728 (2000).
22. P.A. Whitelock, M.W. Feast and F. Van Leeuwen, *Mon. Not. R. Astron. Soc.* **386**, 313 (2008).

23. P.A. Whitelock, J.W. Menzies, M.W. Feast F. Nsengiyumva, and N. Matsunaga, *Mon. Not. R. Astron. Soc.* **428**, 2216 (2013).
24. L.A. Willson, *Ann. Rev. Astron. Astrophys.* **38**, 573 (2000).
25. P.R. Wood, *Astrophys. J.* **190**, 609 (1974).
26. P.R. Wood and D.M. Zarro, *Astrophys. J.* **247**, 247 (1981).
27. P.R. Wood, C. Alcock, R.A. Allsman, D. Alves, T.S. Axelrod, A.C. Becker, D.P. Bennett, K.H. Cook, A.J. Drake, K.C. Freeman, K. Griest, L.J. King, M.J. Lehner, S.L. Marshall, D. Minniti, B.A. Peterson, M.R. Pratt, P.J. Quinn, C.W. Stubbs, W. Sutherland, A. Tomaney, T. Vandehei, D.L. Welch, *Asymptotic Giant Branch Stars*, Ed. by T. Le Bertre, A Lebre, and C. Waelkens, (IAU Symposium 191, 1999), p. 151.
28. P.R. Wood, *Publ. Astron. Soc. Australia* **17**, 18 (2000).
29. W. Yuan, L.M. Macri, A. Javadi, Z. Lin, and J.Z. Huang, *Astron. J.* **156**, 112 (2018).